Research Square

Preprints are preliminary reports that have not undergone peer review.
They should not be considered conclusive, used to inform clinical practice,
or referenced by the media as validated information.

NPC-EVs ameliorate ischemic brain injury by enhancing microglial phagocytosis and anti-inflammatory responses via TREM2-mediated lipid metabolic reprogramming

Lin Zhang
Shanghai Jiao Tong University
Wei Wei
First Affiliated Hospital of Nanchang University
Wenqiang Xin
First Affiliated Hospital of Nanchang University
Guoqiang Hou
Shanghai Jiao Tong University
Xinhang Xu
Shanghai Jiao Tong University
Xiaolan Yang
Shanghai Jiao Tong University
Yaohua Pan
peterpanyaohua@163.com
Shanghai Jiao Tong University
Feng Jia
Shanghai Jiao Tong University
Xiaohua Zhang
Shanghai Jiao Tong University

Research Article

Keywords: ischemic stroke, microglia, NPC-EVs, neuroinflammation, phagocytosis, TREM2

Posted Date: October 14th, 2026

DOI: https://doi.org/10.21203/rs.3.rs-10926953/v1

License: This work is licensed under a Creative Commons Attribution 4.0 International License.
Read Full License

Additional Declarations: No competing interests reported.

Abstract

Inflammation is one of the hallmarks during the pathophysiology of ischemic stroke, among which microglia, as resident immune cells of the brain, play a pivotal role. Despite the latter, recent studies analyzing the precise mechanism by which microglia affect post-stroke neurological outcome remain somewhat limited. Elucidating these mechanisms, however, remains a prerequisite before translational stroke trials are in order. Extracellular vesicles (EVs), significant mediators of intercellular communication, have been demonstrated to possess multiple function of neural repair and neuroregeneration in the pathogenesis and progression of CNS diseases. However, the regulatory role of neural progenitor cell-derived EVs (NPC-EVs) on the phagocytic capacity of microglia post-stroke remains elusive. Using an in vitro stroke model, NPC-EVs effectively drive cultured microglia towards an anti-inflammatory phenotype. Such morphological changes correlate with distinct functional properties of these microglia, which show reduced secretion patterns of pro-inflammatory cytokines and chemokines. In line with this, secretion patterns of anti-inflammatory products are significantly increased, facilitating the efficiency of microglial phagocytosis dependent on TREM2-centric pathways in an in vitro stroke model. NPC-EVs mitigate neuroinflammation and neuronal apoptosis via modulating microglial lipid metabolism, yielding improved neurological recovery in ischemic stroke mice. This provides a novel paradigm for EV-mediated intercellular communication mechanisms and suggests a promising therapeutic potential for NPC-derived EVs in the treatment of ischemic stroke.

Introduction

Ischemic stroke (IS) is not only a consequence of acute vessel occlusion with a lack of oxygen and high-energy phosphates but also implies a complex inflammatory response. The latter exacerbates secondary brain injury, contributing to neural cytotoxicity, oxidative stress, and mitochondrial disturbances. These injuries, in turn, result in brain edema, enhanced neuronal cell apoptosis, and disruption of the blood-brain barrier (BBB). Such inflammation-induced changes affect the peri-infarct area, which subsequently becomes engulfed into the infarct core [1–4]. Targeting inflammatory signaling cascades is therefore currently under investigation as a possible treatment paradigm under stroke conditions [5–9]. However, the interactions between innate immune cells, adaptive immune cells, and brain-intrinsic cells are not well understood under conditions of stroke.

During the early phases of cerebral ischemia, the immune system operates in a coordinated manner, integrating components of both innate and adaptive immunity. This concerted response mirrors immune mechanisms observed in peripheral tissues, contributing to systemic inflammation and localized immune activity [10]. However, the stabilization of ischemic lesions within a few days limits the development of a full-fledged adaptive immune response, emphasizing the predominance of innate immune mechanisms in the acute phase. Microglia, the resident immune cells of the central nervous system, are pivotal in orchestrating the initial inflammatory response during acute ischemic stroke [11]. Their activation, driven by ischemia-induced damage-associated molecular patterns (DAMPs) and cellular debris, initiates a rapid inflammatory cascade. This cascade leads to the release of excitotoxic

agents like glutamate and pro-inflammatory cytokines, including TNF-α, IL-1β, and IL-6, which exacerbate blood-brain barrier (BBB) disruption, neuronal injury, and brain parenchymal damage within minutes to hours post-ischemia [12–14]. Importantly, recent studies underscore the dual role of microglia in ischemic stroke. While their acute activation can potentiate neuroinflammation and secondary injury, their immunomodulatory functions are critical in tissue repair and recovery during later stages [15]. Therefore, targeting microglia-dependent neuroinflammatory pathways offers a promising therapeutic strategy to mitigate acute neuronal damage and promote post-stroke recovery [15]. Furthermore, the intricate interplay between neuroinflammation and immune regulation highlights the necessity of understanding ischemic stroke as not merely a vascular event but also an immune-mediated condition, with implications for designing targeted immunomodulatory interventions [16].

Extracellular vesicles (EVs) constitute a heterogeneous population of vesicles with diameters ranging from 30 to 1000 nm, which encapsulate non-coding RNAs, DNA, and functional proteins including heat shock proteins and tetraspanins [17–19]. Accumulating evidence has demonstrated that EVs derived from stem cells exert therapeutic effects comparable to stem cell transplantation. Although EVs secreted by mesenchymal stem cells (MSCs), neural progenitor cells (NPCs), and other cell types confer partial neuroprotection via modulating immune responses after stroke [20–26], their exact mechanisms of action remain poorly defined. Emerging studies have recently indicated that EVs are capable of regulating microglial activities under both physiological and pathological conditions [22, 27, 28]. Our previous tracking assays validated that immunofluorescent DiI-labeled EVs can be internalized by microglia in the ischemic brain. Nevertheless, how NPC-EV treatment modulates microglial function and subsequently alters immunometabolism and neuroinflammation in the context of ischemic stroke remains largely unexplored. Elucidating these regulatory mechanisms is of great importance, given the prominent functional and metabolic plasticity of microglia; targeting these biological processes via NPC-EV intervention may provide novel insights into stroke therapeutic development. In the present study, we adopted an in vitro microglia-neuron co-culture system and an in vivo murine stroke model to investigate the biological effects of NPC-EVs and their underlying molecular mechanisms. After verifying the regulatory effects of EVs on microglial phenotypes and functions, we further explored the modulatory roles of NPC-EVs in TREM2 protein expression and lipid metabolism, which is expected to provide more preclinical evidence of EV therapy approaches for the treatment of IS.

Materials and methods

Animals

All animal experiments were performed with governmental approval by the Animal Care and Experiment Committee of the School of Medicine, Shanghai Jiao Tong University for the care and use of laboratory animals. The male C57BL/6J mice (10-week-old, weight 30–40 g; The Jackson Laboratory, Bar Harbor, ME, USA) were housed in a temperature and humidity-controlled room under a standard 12-h light/dark cycle for a minimum of 3 days before MCAO induction and provided free access to food and water.

Middle Cerebral Artery Occlusion (MCAO) model

The induction of transient focal cerebral ischemia was described previously [29]. Briefly, animals were under anesthesia with 2% isoflurane and 0.8 L/min O_2. The right common carotid artery was isolated. Subsequently, a 6 – 0 nylon silicon-coated monofilament (diameter 220 ± 20 μm, Doccol Corporation, Massachusetts, USA) was inserted. The filament was carefully advanced towards the MCA and left in place for 60 min. After the designated period, the filament was removed, and the surgical wounds were meticulously sutured. Throughout the procedure, the occlusion and subsequent reperfusion were continuously monitored using laser Doppler flowmetry (LDF). The mice were exposed to MCAO followed by administration of normal saline and EVs (from equivalent 2 x 10^5 NPCs, 10 μg/200 μl) via femoral vein injections at the onset of reperfusion and at 6 h, 24h, and 3d post-MCAO. This optimal EV concentration in vivo was chosen according to previous studies from our group. For the sham group, animals underwent the very same procedure except for insertion of the nylon filament and were given the saline administration at the same time points. At 7-day and 21-day post-MCAO, all mice were humanely sacrificed, and their brain samples were collected for Western blotting and immunofluorescence staining.

EV enrichment from cultured NPCs

The NPC preparation and EV enrichment were based on the method of Zheng et al [24]. Briefly, C57BL/6J mouse pups at postnatal day 0–2 were decapitated and whole brains removed and placed in HBSS on ice. Thereafter, the subventricular zone (SVZ) was dissected in cold PBS under microscopic control, followed by spinning down tissue chunks at 200 x g for 1 min at 4°C. The pellet was suspended and incubated with 0.05% trypsin for 15 min. Each cell pellet was resuspended with NPC culture medium (DMEM/F12 with B27, L-glutamine, 1% penicillin/streptomycin, 20 ng/ml of FGF-2, and 20 ng/ml EGF). The mixture was pelleted by centrifugation at 400 x g for 15 min at room temperature followed by washing steps three times with NPC medium. The resulting pellet was resuspended with NPC medium, and the cells were plated onto the cell culture dish. The neurospheres were observed within 72 h. The cell passage period of NPCs was 5 to 6 days.

After passage 3, NPCs were transferred to T75 flasks with 30 ml NPCs culture medium without growth factors. NPC-conditioned medium (NPC-CM) was collected after 24 h of incubation under standard cell culture conditions. Large vesicles and debris were removed by filtration through 220 nm pore filters (TPP Techno Plastic Products AG, Trasadingen, Switzerland). EVs were enriched from the NPC-CM using the polyethylene glycol (PEG) precipitation method as previously described. In brief, PEG precipitation was performed at a final concentration of 10% PEG 6,000 (50% wt/vol; Merck Group, Darmstadt, Germany) and 75 mM NaCl. After incubation for 12 h at 4°C, the EVs were concentrated by centrifugation for 45 min at 4,500 x g. EVs pellets were dissolved in PBS and precipitated by ultracentrifugation (UC) for 2 h at 110,000 g (Optima XPN-80 Ultracentrifuge, Beckman Coulter, Brea, USA). The EV pellets were resuspended in 500 μl PBS, then which were stored at -80°C until usage. Details about transmission

electron microscopy (TEM), nanoparticle tracking analysis (NTA), and Western blotting of EV markers for EV characterization can be found in **Supplementary Materials and Methods S1**.

Cell Culture

Primary mouse brain microglia were prepared using a previously established protocol [30]. Three C57BL/6J mouse pups at postnatal day 0–2 were decapitated, and whole brains were removed and placed in HBSS. Pooled cortical tissue was digested with 0.25% trypsin and 200 µl of 10 mg/ml DNase at 37°C. After centrifugation, the pellet was gently suspended in 5 mL warm culture media using a 1 mL pipette tip. The homogenous cell suspension was centrifuged at 300 g for 5 min. The resulting pellet was suspended in 20 ml of astrocyte full medium (DMEM supplemented with 10% FBS and 1% penicillin/streptomycin) and cultivated on Poly-D-lysine-coated T75 flasks. The culture medium was changed the next day to remove non-adherent cell debris. After 5–7 days, astrocytes at the bottom of the flask would form a confluent cell layer, and microglia would grow on top of the astrocytic layer. The microglia were collected in conditioned culture medium after vigorously tapping the flasks on the benchtop. A hemocytometer was used to count the floating cell density, and the cells were seeded at 50,000 cells/cm^2 in culture dishes or staining slides for the upcoming experiments.

For the primary cortical neuron cultures, pregnant C57BL/6J mice were sacrificed at embryonic day 16.5. The embryos were then dissected, and cortical tissue pieces were trypsinized and dissociated. Cells were seeded at a density of 100,000 cells per cm^2. On poly-L-ornithine/laminin pre-coated 6-well or 24-well plates (Sigma-Aldrich, St. Louis, MO, USA). Neurobasal medium used for cultures was supplemented (Gibco, NY, USA) with additional transferrin (Sigma-Aldrich, St. Louis, MO, USA), penicillin/streptomycin (PS; Gibco, NY, USA), L-glutamine (Gibco, NY, USA), and B27 supplement (Gibco, NY, USA). The cells were utilized for subsequent experiments following a 4-day period of cell culture.

Primary microglia–neuron co-culture system and treatment

The co-culture model used primary microglia and primary neurons to study the effect of microglia on neuron survival under hypoxic conditions. The experiment was based on the protocol of Skaper et al with some optimizations and modifications [31]. Primary microglia were seeded into a 6-well or 24-well insert (3 µm pore size; Corning, NY, USA) at a density of 50,000 cells/cm^2. After 24-hour treatment, these primary microglia were added to plates pre-seeded with primary neurons respectively, and the co-cultured system would be incubated for another 24 h. Microglia were co-cultured with primary neurons at the start of the reoxygenation of neurons after OGD.

Oxygen-Glucose Deprivation (OGD) model

When the cells reached 80–90% confluence, they were subjected to OGD. To induce OGD, the cells were placed in a BSS0 solution (composed of 116 mM NaCl, 5.4 mM KCl, 0.8 mM MgSO4, 1 mM $NaH_2PO_4H_2O$,

26.2 mM $NaHCO_3$, 10 mM HEPES, 0.01 mM glycine, and 1.8 mM $CaCl_2$, pH 7.2–7.4) and transferred to a hypoxia incubator chamber. The hypoxia chamber maintained an atmosphere of 0.2% O_2, 5% CO_2, and 70% humidity (Don Whitley Scientific H135 HEPA Hypoxystation, England, UK). Following the OGD period, the cells were reoxygenated (RO) by removing the BSS0 solution and placing them in regular cell culture medium. The cells were incubated under standard cell culture conditions (5% CO_2, 37°C) for 24 h before subsequent experiments were performed. In the case of a co-culture system involving primary microglia and cortical neurons, the OGD duration was set at 8 hours, considering the specific tolerance of different cell types to hypoxic injury.

Immunohistochemistry and Immunocytochemistry Staining

Brain samples were fixed overnight in 4% paraformaldehyde. Subsequently, they were dehydrated with 30% sucrose and prepared in 16-μm cryostat sections. To block nonspecific binding, the brain sections were treated with a buffer containing 2% BSA (bovine serum albumin), 10% DS (donkey serum), and 0.25% Triton X-100 in PBS-T. Primary antibodies, such as CD206, were then applied and allowed to incubate overnight. Following this, the sections were treated with appropriate secondary antibodies labeled with Cy-3 or Alexa Fluor 488 (Jackson ImmunoResearch, Ely, UK) for 1 h. Subsequently, 4', 6-diamidino-2-phenylindol (DAPI) staining was performed to visualize the nuclei (dilution: 1 μg/ml in PBS/TBS; Invitrogen, NY, USA). For cell samples, slides or wells were fixed with 4% paraformaldehyde and blocked using 10% DS and 1% BSA in PBS-T. Primary antibodies (Tuj-1, NeuN, Iba1, CD68, CD206, or caspase-3) were incubated with the cells after blocking. Detailed information on specific antibody dilutions can be found in the **Supplementary material resources Table 1**.

To detect cell death rates, terminal deoxynucleotidyl transferase dUTP nick end labeling (TUNEL) staining was performed using the In Situ Cell Death Detection Kit (Merck Group, Darmstadt, Germany), following the manufacturer's instructions. Additionally, 4',6-diamidino-2-phenylindole (DAPI) staining was employed to label the nuclei. In the striatum, a region of interest (ROI), five images were captured per hemisphere. Similarly, for cell samples, five images were taken per well using the Axioplan 2 fluorescence microscope (Carl Zeiss, Jena, Germany). Cell counting and intensity quantification were performed using ImageJ software (National Institutes of Health, USA).

Analysis of phagocytosis

The analysis of microglial phagocytosis refers to the report of Hu et al with modification [32]. Wild type or MNKO microglia were seeded on 4-well chambers (4×10^4 cells/well; Thermo Fisher Scientific, NY, USA) and exposed to OGD treatment for 8 h. Nile red fluorescent microspheres (0.02 μm, Invitrogen, Germany) were dissolved in cell culture medium according to the instructions of the supplier. Cells were incubated with or without microspheres for 4 h. In order to extinguish the signal interference of the extracellular fluorescent microspheres, cells were then washed two times with PBS before fixation and permeabilization, then incubated with specific primary and secondary antibodies. Nuclei were stained

with DAPI. Immunofluorescence slides were photographed with a Zeiss Axioplan 2 fluorescence microscope (Carl Zeiss, Jena, Germany).

Cytotoxicity Assays

The colorimetric assay is suitable for high-throughput quantification of cell death and cell lysis, based on measurement of lactate dehydrogenase (LDH) activity released from the cytosol of damaged cells. The amount of released LDH from cells was measured to reflect levels of cytotoxicity. Following the manufacturer's instructions, a microplate reader was used to examine the absorbance at 490 nm.

Quantitative Real-time Polymerase Chain Reaction (qRT-PCR)

The gene expressions of transfected microglial cells were quantified. Total RNA was extracted using TRIzol reagent (Invitrogen, NY, USA). The KAPA SYBR® FAST One-Step Kit for LightCycler®480 (Merck Group, Darmstadt, Germany) was used for qRT-PCR. The primers (IL-1β, IL-10, TNF-α, and TGF-β1) were purchased from Sangon Biotech (Shanghai, China). The relative quantity levels were calculated with the $2^{-\Delta\Delta Ct}$ method using β-actin as the internal standard control. The reported results are based on three independent experiments on separate batches of cells. The above primer sequence can be found in the **Supplementary Table 2**.

Western Blotting Analysis

Samples were treated for 10 min in a lysate buffer containing 50 mM Tris, 1% Triton-X 100, 131 mM sodium chloride, 1 mM sodium diphosphate, 1 mM sodium fluoride, 1 mM EDTA, 1% protease inhibitor, and 1% phosphatase inhibitor with a homogenisator, followed by 10 min at 16,000 rpm centrifuge at 4°C. The protein concentration of supernatant was quantified using Pierce™ BCA Protein Assay Kit (Thermo Fisher Scientific, NY, USA). The samples with reducing sample buffer (Thermo Fisher Scientific, NY, USA) were heated for 5 min at 95°C. Equal amounts of proteins were added to 8–12% SDS-PAGE and then transferred onto a nitrocellulose membrane (Bio-Rad, Hercules, California, USA). The membranes were blocked for 1 h and incubated with the primary antibodies Alix, CD63, TSG101, LRP1, MerTK, CX3CR1, TREM2, LXRα, ABCA1, Bax, Bcl-2, caspase-3, and cleaved caspase-3 overnight. The blots were washed with tris-buffered saline supplemented with 0.1% Tween® 20 detergent (TBS-T) three times, then incubated with a horseradish peroxidase-coupled secondary antibody (1:10,000) for 1 h. The specific antibody working dilutions are given in the resources table in the supplementary material. The membranes were reserved in ECL reagent and subsequently imaged with a Bio-Rad system (ChemiDoc™ XRS+).

Analysis of post-stroke motor coordination deficits

To ensure appropriate test behavior, the mice underwent training sessions for 2 consecutive days prior to stroke induction. The assessment of motor coordination was carried out at specific time points (pre-stroke day 1 and post-stroke day 3, 7, and 21) using well-established tests, including the rotarod test,

tightrope test, balance beam test, and corner turn test, as described in previous studies [33, 34]. Each test day involved three repetitions of the rotarod, balance beam, and tightrope tests, with the mean values computed for analysis. In the rotarod test, the measured parameter was the duration until the mice fell off, with a maximum testing time of 300 seconds. Similarly, in the balance beam test, the parameter recorded was the time taken by the mice to reach the platform, with a maximum testing time of 60 seconds. The evaluation of the tightrope test outcomes was conducted using a validated scoring system that ranged from 0 (minimum) to 20 (maximum). Specific sheet regarding the tightrope test scores can be found **Supplementary Table 3**. In the corner turn test, 10 trials were performed per test day, and the laterality index (number of right turns out of 10 trials) was calculated. Higher laterality indexes, approaching a score of 1, indicated pronounced motor coordination impairment.

Lipid Sample Preparation

The extraction was using a modified Folch lipid extraction procedure as following: The lipid was extracted from 100μL serum using 300 μL chloroform: methanol (2:1, v/v) contained known amounts of isotope-labeled internal mix standards, vortex for 30 s and ultrasonic extraction for 10 min, then holding 30 min at -20°C and transfer chloroform layers about 200 μL into a centrifuge tube after centrifugation 10 min at 13000 rpm and 4°C. The residue was reextracted under the same conditions as above. Then combine the chloroform layers and lyophilize in a centrifugal vacuum evaporator at 4°C. Finally, samples were reconstituted in isopropanol: methanol (1:1, v/v), vortexed for 30 s, ultrasonically extracted for 3 min, centrifuged for 10 min at 13,000 rpm, and stored at − 20°C before LC-MS analysis. The QC samples were prepared by mixing aliquots of all the samples to form a pooled sample.

LC-MS/MS Analysis

The metabolomic data analysis was performed by Shanghai Luming Biological Technology Co., Ltd. (Shanghai, China). The LC system was performed using an ExionLC™ System consisting of a binary high-pressure mixing gradient pump with degasser, a thermostated autosampler, and a column oven, and the MS was QTRAP 6500+ (AB Sciex, USA) equipped with an IonDrive™ Turbo V source. LC-MS/MS data were processed by Hiroshi, RIKEN Center for Sustainable Resource Science MRMPROBS. The quantitative analysis of different types of lipids was carried out. The resulting matrix was further reduced by removing any peaks with a missing value (ion intensity = 0) in more than 50% samples. The internal standard was used for data QC. The positive and negative data were combined to get a combined dataset, which was imported into the R ropls package. Principal component analysis (PCA) and (orthogonal) partial least-squares-discriminant analysis (O)PLS-DA were carried out to visualize the metabolic alterations among experimental groups, after mean centering and Pareto variance scaling, respectively. The Hotelling's T2 region, shown as an ellipse in score plots of the models, defines the 95% confidence interval of the modeled variation. Variable importance in the projection (VIP) ranks the overall contribution of each variable to the OPLS-DA model, and those variables with VIP > 1 are considered relevant for group discrimination.

In the present study, the default 7-round cross-validation was applied, with 1/seventh of the samples being excluded from the mathematical model in each round, to guard against overfitting. The differential metabolites were selected based on the combination of a statistically significant threshold of VIP values obtained from the OPLS-DA model and p-values from a two-tailed Student's t-test on the normalized peak areas, where metabolites with VIP values larger than 1.0 and P-values less than 0.05 were considered as differential metabolites. Differential metabolites were further used for KEGG pathway enrichment analysis.

Statistical Analysis

All data were expressed as means ± standard deviation (SD). To compare two groups, the Student's t-test was employed for statistical analysis. For comparisons among multiple groups, a one-way analysis of variance (ANOVA) or a two-way ANOVA for factorial comparisons was utilized. Post hoc tests, such as Bonferroni or Tukey-Kramer's test, were applied for multiple comparisons. Statistical significance was considered when p-values were less than 0.05. The statistical analyses were performed using GraphPad Prism 6.0 software (GraphPad, San Diego, CA, USA).

Results

Purification, Isolation, and Characterization of NPC-EVs

Primary NPCs were isolated from the mouse subventricular zone, and NPC-EVs were enriched by using established PEG method (Fig. 1A) [35]. The subsequent characterization of such enriched NPC-EVs included Western blot of EV biomarkers, transmission electron microscopy (TEM), and nanoparticle tracking analysis (NTA). EV enrichment revealed the presence of commonly reported EV biomarkers such as Alix, CD63, and Tsg101 compared with NPC cell lysate groups (Fig. 1B). Transmission electron microscopy analysis showed cup-shaped EVs from conditioned medium of NPCs (Fig. 1C). NPC-EVs were further quantified and evaluated for size using NTA, which displayed an EV-like spectrum. The distribution patterns from the NTA results revealed the majority of NPC-EVs to be at about 50 to 150 nm in size (Fig. 1D-E). According to the above results, we applied the PEG method to enrich NPC-EVs for the remainder of the study efficiently.

Extracellular vesicles (EVs) derived from NPCs (NPC-EVs) preserved neurological function and reduced neuroinflammation in a murine stroke model.

NPC-EVs were proven to have neuroprotective effects in pre-clinical studies [24, 25]. We further investigated whether NPC-EVs improve neurological recovery at multiple time points after cerebral ischemia in mice. Delivery of these EVs resulted in significantly better test performance of the animals in the rotarod test, balance beam test, tightrope test, as well as in the recording of corner turn test on days 7 and 21 when compared with MCAO treated with vehicle control groups. However, these beneficial effects were not immediately visible on day 3 after stroke induction, indicating a time-dependent process for EV-induced neuroprotection (Fig. 1F). Taken together, the behavior test results indicate that EV

treatment significantly prevents postischemic motor coordination impairment in non-acute phase after stroke. By measuring inflammatory cytokines of cerebral tissue homogenate, EV administration significantly increased anti-inflammatory cytokines (TGF-β1, IL-10), and reduced pro-inflammatory cytokines (TNF-α, IL-1β) compared to the vehicle treatment in stroke mice (Fig. 1G). These results suggested that the delivery of EVs derived from NPCs improve neurological recovery, which may be ascribed to inhibiting the inflammatory response in the infarcted area.

Transcriptomic analysis unveiled NPC-EVs regulate microglia pathogen phagocytosis pathway against post-ischemic inflammation.

In the MCAO ischemia model, RNA-seq analysis of ipsilateral brain tissues from EV treated and vehicle treated stroke mice revealed significant transcriptional differences, particularly in immune and inflammation-related pathways by KEGG pathway analysis (Fig. 2A-B). WikiPathways enrichment analysis highlighted the upregulation of the 'Microglia pathogen phagocytosis pathway' (WP3626) in the ischemic mice treated with EVs compared to vehicle control groups (Fig. 2C-D), suggesting enhanced microglial phagocytic activity upon EV administration. Key genes driving this enrichment included Trem2 (triggering receptor expressed on myeloid cells 2), Tyrobp (TYRO protein tyrosine kinase binding protein, also known as DAP12), Fcer1g (Fc fragment of IgE receptor subunit gamma), Rac2 (Ras-related C3 botulinum toxin substrate 2), and Ptpn6 (protein tyrosine phosphatase non-receptor type 6), all of which are critical for microglial phagocytosis (Fig. 2E). The heatmap further confirmed the elevated expression of these genes, with Trem2 and Tyrobp/DAP12 emerging as potential master regulators of microglial phagocytic function (Fig. 2F). Additional pathways, such as 'Macrophage marker,' 'Tyrobp causal network in microglia,' and 'IL-3 signaling pathway,' also showed differential regulation, implicating broader immune modulation by EV treatment (Fig. 2C). Notably, PI3K-Akt-mTOR signaling components (Pik3cg, Pik3cd, Pik3r1, etc.) were enriched, suggesting their potential role in linking EV treatment to inhibit inflammatory response against ischemic injury. EV administration elevated TREM2 expression on days 7, 14, and 21 after stroke, in agreement with the trend of anti-inflammatory cytokines of cerebral tissue homogenate compared to the vehicle treatment in stroke mice (Fig. 3A). These findings demonstrate that EV delivery may reshape the ischemic brain’s transcriptomic landscape in 7 days after stroke in the C57BL/6 mice, promoting microglial phagocytosis through TREM2-centric pathways.

NPC-EVs modulated polarization of microglia, neuron apoptosis, and neuroinflammation in stroke mice.

To confirm the protective effects of NPC-EV administration and the underlying mechanism in the ischemic stroke animal model, we further investigated the impact of EVs on polarization patterns of microglia and on neuroinflammation in stroke mice. Immunofluorescence staining identified significantly more CD206 labelled microglia around the infarct area, indicating a shift towards an anti-inflammatory M2 microglia polarization (Fig. 3B, D). Furthermore, we found that MCAO triggered a significant increase in the expression of both pro-inflammatory and anti-inflammatory responses compared to the sham group in both vehicle and EV treated mice. However, the qRT-PCR analysis revealed a reduction in pro-

inflammatory TNF-α and IL-1β levels, accompanied by a significant increase of the anti-inflammatory factors IL-10 and TGF-β1 post-stroke in EV treated mice compared to the vehicle group (Fig. 3F-I). Of note, TUNEL staining within the ischemic striatum revealed 56% less TUNEL-positive cell counts (Fig. 3C, E) post-MCAO in the EV treated group compared with the vehicle control group. Taken together, EV treatment induced microglial anti-inflammatory M2 polarization, which protects neurons against apoptosis in 7 days post-stroke mice.

NPC-EVs drove microglia towards an M2-like phenotype and suppressed neuroinflammation in the microglia/neuron co-culture OGD model.

To explore the impact of EV delivery on the function of microglia and subsequent immunometabolism, we generated an in vitro microglia/neuron co-culture system that mimics the stroke conditions found in the intact organism (Fig. 4A-B). Since microglia respond to various stimuli after stroke, yielding either tissue damage or repair [36, 37], we first explored polarization patterns by co-labelling of the microglia marker Iba1 with the M2 phenotype marker CD206 (Fig. 4C-D). As such, the number of CD206-positive microglia was about a 40% increase in the co-culture group with EV treatment when compared to the vehicle control group under OGD conditions (n = 5). Considering M2 microglia exist in an anti-inflammatory state and secrete anti-inflammatory cytokines to promote brain repair, we further compared both the pro- and anti-inflammatory cytokines in the co-culture model with EV treatment post OGD with the vehicle control group. Our data showed a significant reduction of the pro-inflammatory cytokines TNF-α and IL-1β in the EV treated group under OGD conditions. On the other hand, the production of typical anti-inflammatory factors like IL-10 and TGF-β1 increased by about 50% in the EV treated co-culture post-OGD group in comparison to the vehicle control group (Fig. 4E-H). Hence, in our in vitro results, these findings revealed EVs promoted microglial M2 anti-inflammatory polarization and attenuated post-OGD inflammation in the microglia/neuron co-culture model.

NPC-EVs facilitated microglial efferocytosis in the microglia/neuron co-culture OGD model.

Efferocytosis is a pivotal mechanism of clearance of unnecessary cells and cell debris in the central nervous system. Further reports also suggest the potential role of microglial efferocytosis in neuroprotection via maintaining tissue homeostasis, modulating inflammation, and facilitating tissue repair [38–40]. We therefore evaluated the scale of efferocytosis in microglia after OGD treatment. The proportion of Nile red-positive microglia (phagocytosing fluorescent microspheres) increased by nearly 40% in the EV-treated group compared with the vehicle control group (Fig. 5A-C). To confirm elevated microglial efferocytosis, the expression of the efferocytotic process-dependent proteins LRP1, MerTK, and CX3CR1 was significantly up-regulated (Fig. 5D-E) corresponding to above results of immunofluorescence staining. Taken together, our results indicate a dramatic enhancement of microglial efferocytosis, facilitating tissue repair in the EV-treated group after OGD.

NPC-EVs reduced neuronal damage by inhibiting apoptosis and cytotoxicity in the co-culture OGD model.

We then investigated whether these pronounced changes in anti-inflammation and efferocytosis might translate to a gain of reduced neuronal apoptosis and attenuated cytotoxicity. To address this question, we performed TUNEL/NeuN co-staining and a lactate dehydrogenase (LDH) assay, which provides a method for determining neuronal cytotoxicity. Our results revealed 33% less TUNEL/NeuN positive cell counts in the EV-treated group compared to the vehicle control group in the co-culture OGD model (Fig. 6A-B). Additionally, we observed a 10% reduction of LDH release (Fig. 6E-F) after OGD induction in the EV-treated group compared with the vehicle control group, suggesting a decrease in cytotoxicity. To gain a more comprehensive understanding of the extent and breadth of reduced neuronal apoptosis mediated by EV delivery, we evaluated the expression of Bax/Bcl-2 and cleaved caspase-3/caspase-3 (Fig. 6C-D), indicating a significant reduction in neuronal apoptosis. Our data showed that the number of neurons stained with both caspase-3 and Tuj-1 significantly decreased in co-cultures with EV-treated microglia. Furthermore, the expression ratios of Bax/Bcl-2 and cleaved caspase-3/caspase-3 showed a remarkable decline in the EV-treated group compared the vehicle control group (Fig. 6G-I). These results strongly implicate a correlation of reduced neuronal apoptosis and attenuated cytotoxin release with anti-inflammation and efferocytosis changes in neurons co-cultured with EV-treated microglia under OGD conditions.

TREM2 mediates NPC-EV-driven remodeling of microglial lipid metabolism and functional phenotypes in ischemic mouse brains

Immunofluorescent staining revealed prominent intracellular lipid droplet deposition within iNOS + pro-inflammatory microglia localized to the infarct core (Fig. 7A). In the present study, our findings demonstrated that insufficient TREM2 may play a critical part in ischemic brain, which impaired microglial function including anti-inflammation and phagocytosis via increasing lipid droplet accumulation and deteriorating cellular cholesterol homeostasis (Fig. 7B). We further demonstrated the molecular and metabolic consequences of EV delivery on TREM2-mediated microglial function and lipid metabolism in ischemic stroke. Lipidomic profiling was performed to characterize lipid metabolite shifts induced by NPC-EV intervention. Multiple triglyceride (TAG) subtypes (TAG54:3 (16:0), TAG52:1 (18:0), TAG52:1 (16:0)), phosphatidylcholines (PC (16:0/16:0), PC (16:0/18:1)), phosphatidylethanolamines (PE (18:1p/22:4), PE (18:0p/22:6)), sphingomyelin SM (d18:1/22:0) and lysophosphatidylcholine LPC (18:0) exhibited statistically significant alterations in abundance following NPC-EV treatment (Fig. 7C). KEGG pathway enrichment further validated that NPC-EVs predominantly modulate microglial cholesterol metabolic cascades among all lipid-related pathways (Fig. 7D). Stereotactic injection of trem2-targeted siRNA successfully knocked down cerebral TREM2 expression in both vehicle- and NPC-EV-treated stroke mice, as validated by western blot (Fig. 7E-F). TREM2 knockdown markedly downregulated LXRα protein abundance in both experimental cohorts. Conversely, NPC-EV administration upregulated TREM2 protein in ischemic brain tissue, which subsequently activated LXR signaling to elevate the cholesterol efflux transporter ABCA1 (Fig. 7F-G). Quantification of intracellular cholesteryl ester content confirmed that NPC-EVs rescued the lipid overload triggered by ischemic injury and TREM2 ablation (Fig. 7H). Dual

immunofluorescence co-staining of BODIPY-labeled lipid droplets (green), the pro-inflammatory marker iNOS (red) and DAPI nuclear counterstain demonstrated robust lipid droplet accumulation in vehicle-treated microglia, reflected by elevated BODIPY mean fluorescence intensity (MFI). While TREM2 knockdown drastically increased BODIPY MFI, NPC-EV intervention partially counteracted this lipid overload even under TREM2 knockdown conditions. In parallel, iNOS expression was markedly augmented after Trem2 siRNA delivery; NPC-EVs substantially attenuated TREM2 depletion-induced iNOS upregulation (Fig. 7I, 7J). Western blot quantification of lipid and apoptosis-related proteins yielded consistent molecular evidence. The lipid droplet structural protein PLIN2 was significantly accumulated upon TREM2 knockdown, an effect effectively reversed by NPC-EV treatment. Moreover, TREM2 knockdown shifted the apoptotic balance toward pro-death signaling via elevated BAX and suppressed Bcl-2 levels, whereas NPC-EV administration restored anti-apoptotic Bcl-2 expression and alleviated neuronal apoptotic injury (Fig. 7K, 7L). Collectively, these multi-omics, imaging and immunoblot data demonstrate that NPC-EVs upregulate microglial TREM2 to activate the TREM2/LXR/ABCA1 axis. This signaling cascade normalizes disordered cholesterol and lipid metabolism, suppresses pro-inflammatory microglial polarization, and stabilizes neuronal anti-apoptotic signaling in the ischemic brain.

Discussion

Using both in vitro and in vivo ischemic stroke models, the present work delineates a novel regulatory mechanism by which neural progenitor cell-derived extracellular vesicles (NPC-EVs) improve long-term neurological recovery via remodeling microglial immunometabolism and suppressing neuronal injury. Consistent with prior reports, microglial lipid homeostasis is a core switch governing neuroinflammatory activity: inhibiting lipid accumulation curbs the secretion of pro-inflammatory cytokines (TNF-α, IL-1β) while elevating anti-inflammatory mediators IL-10 and TGF-β1 [41–43]. Our data further clarify that NPC-EVs do not exert direct inhibitory effects on hypoxia-triggered inflammatory cascades; instead, they target the TREM2/LXR/ABCA1 signaling axis to modify microglial lipid metabolism, thereby conferring anti-inflammatory and neuroprotective effects. These results align with previous studies and establish NPC-EVs as a promising therapeutic agent to drive microglia toward a reparative phenotype in ischemic stroke.

Persistent inflammatory responses within the peri-infarct penumbra constitute a critical driver of progressive neuronal deterioration following ischemic stroke, which ultimately undermines long-term neurological functional recovery [44–46]. The penumbra, defined as the hypoperfused yet viable tissue surrounding the core infarct, continuously releases damage-associated molecular patterns (DAMPs) post-ischemia, thereby sustaining protracted neuroinflammatory cascades that extend beyond the acute phase into the subacute and chronic stages. This sustained inflammatory milieu exacerbates blood-brain barrier breakdown, impairs synaptic plasticity, halts myelin regeneration, and gradually depletes surviving neurons in the penumbral region, culminating in irreversible permanent neurological deficits [47–49]. As the primary resident myeloid immune sentinels of the central nervous system, microglia act as the central orchestrator of penumbral inflammation. Imbalanced microglial polarization and metabolic dysfunction in the mid-to-late stroke period fuel the establishment of a pro-inflammatory niche:

classically activated pro-inflammatory microglia robustly secrete TNF-α, IL-1β and IL-6 to amplify inflammatory infiltration, whereas the population of reparative microglia with efferocytic and anti-inflammatory capacities progressively declines, creating a self-perpetuating vicious cycle of unresolved inflammation and impaired tissue repair [47, 50]. Multiple transcription regulators including NF-κB, STAT3 and PPARγ have been implicated in controlling microglial polarization states, as documented in previous transcriptomic studies [51–55].

Under physiological conditions, ramified surveillant microglia continuously monitor CNS tissue homeostasis. Upon ischemic injury, microglia undergo functional polarization into two distinct subsets: pro-inflammatory M1 microglia that exacerbate neuronal damage, and anti-inflammatory M2/reparative microglia that resolve inflammation and facilitate brain repair [44, 56]. M2 microglia secrete trophic factors such as VEGF, MMP-9 and TGF-β1 to support angiogenesis, extracellular matrix remodeling and neuronal survival; accordingly, therapeutic strategies shifting microglia toward the reparative phenotype have attracted extensive research interest for stroke intervention [47, 48, 57]. Building on this framework, our study focuses on subacute and chronic stroke stages, with microglia defined as the primary cellular effector of MSC/NPC-EV bioactivity [58, 59]. Internalized by penumbral microglia, EVs deliver cargo comprising non-coding RNAs, lipid mediators and neurotrophic proteins to reshape microglial transcriptional and metabolic profiles [60]. Mechanistically, NPC-EVs upregulate the reparative receptor TREM2 and activate downstream LXR/ABCA1 signaling, thereby correcting pathological lipid accumulation and augmenting microglial efferocytosis. This phenotypic transition toward anti-inflammatory microglia remodels the penumbral niche into a regenerative microenvironment. Distinct from anti-inflammatory interventions targeting the acute stroke window, NPC-EVs exert sustained modulatory effects on the chronic inflammatory signature specific to mid-to-late stroke lesions, sustaining the reparative potential of penumbral parenchyma and interrupting the pathological loop linking persistent neuroinflammation to poor long-term prognosis.

TREM2/LXR/ABCA1 signaling represents a key downstream effector mediating NPC-EV-induced microglial reprogramming. Accumulated evidence confirms TREM2 as a master controller of microglial efferocytosis, which eliminates apoptotic cell debris to avoid secondary inflammatory stimulation [69,71,72]. Liver X receptors (LXRs) constitute ligand-activated nuclear receptors functioning downstream of TREM2. As master transcriptional regulators, LXRs sense intracellular lipid homeostasis, coordinate inflammatory gene programmes, and govern the phagocytic capacity of myeloid cells[61, 62]. Efferocytosis is essential for resolving inflammation and preventing secondary damage caused by the accumulation of apoptotic cells and the subsequent release of pro-inflammatory mediators [69, 71, 72]. TREM2 activation has been validated to enhance phagocytic capacity, suppress inflammatory transcription, and alleviate neurological injury across multiple neurodegenerative and cerebrovascular diseases [63–65]. Our results verify that NPC-EVs rely on TREM2/LXR/ABCA1 signaling to restore microglial homeostatic function, though the direct or indirect regulatory crosstalk between NPC-EVs and TREM2 expression/activity requires further validation. Additional transcriptional axes including NF-κB and PPARγ also participate in microglial functional tuning and may cooperate with the TREM2-lipid regulatory cascade uncovered here [66, 67].

Lipid metabolic reprogramming serves as a master determinant governing the functional identity of microglia during the subacute and chronic phases of ischemic stroke [68]. Following cerebral ischemia, aberrant lipid trafficking and excessive intracellular lipid droplet deposition in penumbral microglia disrupt their efferocytic competence and anti-inflammatory transcriptional program, locking these cells into a dysfunctional, pro-inflammatory state that perpetuates sustained neuroinflammation and impedes endogenous brain repair cascades, ultimately compromising long-term neurological rehabilitation outcomes [69]. The present study demonstrates that NPC-EVs reverse microglial lipid dysfunction by activating the TREM2-DAP12 signaling cascade. TREM2 signaling transcriptionally upregulates lipid catabolic genes (LIPA, APOE, GPNMB) and suppresses lipid uptake/storage transcripts, alleviating pathological lipid overload and lipid-mediated cellular stress [70, 71]. Metabolic normalization driven by TREM2 signaling further drives a phenotypic switch of microglia toward the IGF1-high reparative subset characterized by robust efferocytosis, restrained secretion of TNF-α and IL-1β, and elevated expression of multiple neurotrophic factors [72]. By resolving lipid metabolic disorder via TREM2-dependent homeostatic control, NPC-EVs interrupt the post-stroke pathological loop of lipid overload-dysfunctional microglia-chronic inflammation, promoting synaptic reconstruction and remyelination in the penumbra and achieving durable functional recovery. The current work thus delineates a novel NPC-EV/TREM2/lipid metabolism regulatory axis linking myeloid metabolic plasticity to brain tissue repair, highlighting TREM2/LXR/ABCA1 signaling as a druggable checkpoint to reverse lipid-mediated microglial dysfunction in subacute and chronic ischemic stroke, and supporting the translational potential of NPC-EVs as a vesicle-based therapeutic modality targeting microglial immunometabolism.

This study substantiates the neuroprotective efficacy of NPC-EVs against ischemic stroke. Mechanistically, NPC-EVs activate TREM2/LXR/ABCA1 signaling to normalize microglial lipid metabolism, facilitate the shift toward reparative microglia, boost efferocytic clearance, mitigate sustained neuroinflammation and neuronal apoptosis. Microglia serve as the primary cellular mediator through which NPC-EVs alleviate subacute and chronic neuroimmune dysfunction and improve long-term stroke outcomes. These findings provide novel mechanistic insights and support the translational prospect of NPC-EV-based therapies; future research can further optimize brain-targeted NPC-EV delivery systems to extend the therapeutic window for stroke rehabilitation.

Conclusion

Our study demonstrates that NPC-derived extracellular vesicles (NPC-EVs) exert sustained neuroprotective effects after ischemic stroke by reprogramming microglial immunometabolism. NPC-EVs upregulate microglial TREM2 and activate the downstream LXR/ABCA1 pathway, thereby restoring disrupted lipid and cholesterol homeostasis and reducing pathological lipid accumulation. This metabolic reprogramming promotes a reparative microglial phenotype and enhances efferocytic clearance, accompanied by reduced pro-inflammatory responses and neuronal apoptosis. Importantly, TREM2 deficiency substantially impaired these beneficial effects, supporting the critical role of TREM2-centered signaling in NPC-EV-mediated microglial functional remodeling. Collectively, our findings identify the NPC-EV/TREM2/LXR/ABCA1 axis as a potential regulatory mechanism linking microglial

lipid metabolism to resolution of post-stroke neuroinflammation and tissue repair. These findings further support NPC-EVs as a promising cell-free therapeutic strategy for improving neurological recovery after ischemic stroke and provide a rationale for future studies aimed at optimizing EV delivery and therapeutic efficacy.

Abbreviations

Nonstandard Abbreviations and Acronyms	
NPCs	neural progenitor cells
EVs	Extracellular vesicles
WT	wild type
TREM2	triggering receptor expressed on myeloid cells 2
LXR	Liver X receptors
IS	ischemic stroke
BBB	blood-brain barrier
DAMPs	damage-associated molecular patterns
CNS	central nervous system
MCAO	middle cerebral artery occlusion
OGD	oxygen-glucose deprivation
TAG	triglyceride
IL-10	interleukin-10
TGF-β1	transforming growth factor-beta 1
TNF-α	tumor necrosis factor-alpha
IL-1β	interleukin-1β
VEGF	vascular endothelial growth factor
MMP-9	matrix metalloproteinase-9
PPARγ	peroxisome proliferator-activated receptor gamma
STAT3	signal transducer and activator of transcription 3
NF-κB	nuclear factor-kappa B
qRT-PCR	quantitative real-time polymerase chain reaction

Declarations

Authors' contributions

LZ, WW, WX, YP, XZ, and FJ conceived the project and designed the experiments. LZ, WW and WX performed the in vitro experiments. XY, GH, XX, YP and FJ performed the in vivo experiments. LZ, XZ, FJ, and YP interpreted the results and stewarded the overall project. LZ, WW, WX, YP, XZ, and FJ co-wrote the manuscript. LZ, XZ, and FJ provided financial support. All authors discussed the results and commented on the manuscript.

Sources of Declaration

This work was supported by the National Natural Science Foundation of China (82301462, 82271310, and 82501593), the Natural Science Foundation of Jiangxi Province (20252BAC200110 and 20262BAC240214), and Science and Technology Commission of Shanghai Municipal (23PJ1407700).

Ethics Approval

All applicable international, national, and/or institutional guidelines for the care and use of animals were followed. This article does not contain any studies with humans performed by any of the authors.

Availability of data and materials

The datasets used and/or analysed during the current study are available from the corresponding author on reasonable request. Supplementary information was listed in the attached supplementary file.

Competing interests

The authors declare that they have no conflicts of interest with the contents of this article.

Acknowledgements

This article does not contain any studies with human participants performed by any of the authors. All animal experiments were performed with governmental approval according to the National Institutes of Health guidelines for the care and use of laboratory animals (YS-m202307001).

Disclosures

None.

References

1. Schilling, M., et al., *Effects of monocyte chemoattractant protein 1 on blood-borne cell recruitment after transient focal cerebral ischemia in mice.* Neuroscience, 2009. **161**(3): p. 806-12.

2. Rosell, A., et al., *Increased brain expression of matrix metalloproteinase-9 after ischemic and hemorrhagic human stroke.* Stroke, 2006. **37**(6): p. 1399-406.
3. Herz, J., et al., *Role of Neutrophils in Exacerbation of Brain Injury After Focal Cerebral Ischemia in Hyperlipidemic Mice.* Stroke, 2015. **46**(10): p. 2916-25.
4. Sorce, S., et al., *Increased brain damage after ischaemic stroke in mice lacking the chemokine receptor CCR5.* Br J Pharmacol, 2010. **160**(2): p. 311-21.
5. Macrez, R., et al., *Stroke and the immune system: from pathophysiology to new therapeutic strategies.* Lancet Neurol, 2011. **10**(5): p. 471-80.
6. Chamorro, Á., et al., *The immunology of acute stroke.* Nat Rev Neurol, 2012. **8**(7): p. 401-10.
7. Iadecola, C. and J. Anrather, *The immunology of stroke: from mechanisms to translation.* Nat Med, 2011. **17**(7): p. 796-808.
8. Amarenco, P., et al., *High-dose atorvastatin after stroke or transient ischemic attack.* N Engl J Med, 2006. **355**(6): p. 549-59.
9. Sacco, R.L., et al., *Aspirin and extended-release dipyridamole versus clopidogrel for recurrent stroke.* N Engl J Med, 2008. **359**(12): p. 1238-51.
10. Iadecola, C., M.S. Buckwalter, and J. Anrather, *Immune responses to stroke: mechanisms, modulation, and therapeutic potential.* J Clin Invest, 2020. **130**(6): p. 2777-2788.
11. Patel, A.R., et al., *Microglia and ischemic stroke: a double-edged sword.* Int J Physiol Pathophysiol Pharmacol, 2013. **5**(2): p. 73-90.
12. Gelderblom, M., et al., *Temporal and spatial dynamics of cerebral immune cell accumulation in stroke.* Stroke, 2009. **40**(5): p. 1849-57.
13. Xiong, X.Y., L. Liu, and Q.W. Yang, *Functions and mechanisms of microglia/macrophages in neuroinflammation and neurogenesis after stroke.* Prog Neurobiol, 2016. **142**: p. 23-44.
14. Belov Kirdajova, D., et al., *Ischemia-Triggered Glutamate Excitotoxicity From the Perspective of Glial Cells.* Front Cell Neurosci, 2020. **14**: p. 51.
15. Jurcau, A. and A. Simion, *Neuroinflammation in Cerebral Ischemia and Ischemia/Reperfusion Injuries: From Pathophysiology to Therapeutic Strategies.* Int J Mol Sci, 2021. **23**(1).
16. Stuckey, S.M., et al., *Neuroinflammation as a Key Driver of Secondary Neurodegeneration Following Stroke?* Int J Mol Sci, 2021. **22**(23).
17. Chitti, S.V., et al., *Vesiclepedia 2024: an extracellular vesicles and extracellular particles repository.* Nucleic Acids Res, 2024. **52**(D1): p. D1694-d1698.
18. Welsh, J.A., et al., *Minimal information for studies of extracellular vesicles (MISEV2023): From basic to advanced approaches.* J Extracell Vesicles, 2024. **13**(2): p. e12404.
19. Abels, E.R. and X.O. Breakefield, *Introduction to Extracellular Vesicles: Biogenesis, RNA Cargo Selection, Content, Release, and Uptake.* Cell Mol Neurobiol, 2016. **36**(3): p. 301-12.
20. Kim, E.H., et al., *Clinical Scale MSC-Derived Extracellular Vesicles Enhance Poststroke Neuroplasticity in Rodents and Non-Human Primates.* J Extracell Vesicles, 2025. **14**(6): p. e70110.

21. Go, V., et al., *Extracellular vesicles from mesenchymal stem cells reduce microglial-mediated neuroinflammation after cortical injury in aged Rhesus monkeys.* Geroscience, 2020. **42**(1): p. 1-17.
22. Zhou, Y., et al., *Mesenchymal-derived extracellular vesicles enhance microglia-mediated synapse remodeling after cortical injury in aging Rhesus monkeys.* J Neuroinflammation, 2023. **20**(1): p. 201.
23. Song, J., et al., *Advancing stroke therapy: innovative approaches with stem cell-derived extracellular vesicles.* Cell Commun Signal, 2024. **22**(1): p. 369.
24. Zheng, X., et al., *Extracellular Vesicles Derived from Neural Progenitor Cells--a Preclinical Evaluation for Stroke Treatment in Mice.* Transl Stroke Res, 2021. **12**(1): p. 185-203.
25. Li, Y. and B. Fang, *Neural stem cell-derived extracellular vesicles: The light of central nervous system diseases.* Biomed Pharmacother, 2023. **165**: p. 115092.
26. Boese, A.C., et al., *Neural stem cell therapy for subacute and chronic ischemic stroke.* Stem Cell Res Ther, 2018. **9**(1): p. 154.
27. Saieva, S., et al., *Hippocampal neural stem cell-derived extracellular vesicles modulate microglia to promote resilience against tau oligomers.* Neural Regen Res, 2026. **21**(9): p. 4424-4434.
28. Madhu, L.N., et al., *Extracellular vesicles from human-induced pluripotent stem cell-derived neural stem cells alleviate proinflammatory cascades within disease-associated microglia in Alzheimer's disease.* J Extracell Vesicles, 2024. **13**(11): p. e12519.
29. Bertrand, L., L. Dygert, and M. Toborek, *Induction of Ischemic Stroke and Ischemia-reperfusion in Mice Using the Middle Artery Occlusion Technique and Visualization of Infarct Area.* J Vis Exp, 2017(120).
30. Lian, H., E. Roy, and H. Zheng, *Protocol for Primary Microglial Culture Preparation.* Bio Protoc, 2016. **6**(21).
31. Skaper, S.D. and L. Facci, *Central nervous system neuron-glia co-culture models and application to neuroprotective agents*, in *Neurotrophic Factors*. 2018, Springer. p. 63-80.
32. Hu, X., et al., *Microglia/macrophage polarization dynamics reveal novel mechanism of injury expansion after focal cerebral ischemia.* 2012. **43**(11): p. 3063-3070.
33. Balkaya, M., et al., *Assessing post-stroke behavior in mouse models of focal ischemia.* J Cereb Blood Flow Metab, 2013. **33**(3): p. 330-8.
34. Doeppner, T.R., et al., *Effects of neural progenitor cells on post-stroke neurological impairment-a detailed and comprehensive analysis of behavioral tests.* Front Cell Neurosci, 2014. **8**: p. 338.
35. Zhang, L., et al., *Neural Progenitor Cell-Derived Extracellular Vesicles Enhance Blood-Brain Barrier Integrity by NF-κB (Nuclear Factor-κB)-Dependent Regulation of ABCB1 (ATP-Binding Cassette Transporter B1) in Stroke Mice.* Arterioscler Thromb Vasc Biol, 2021. **41**(3): p. 1127-1145.
36. Lan, X., et al., *Modulators of microglial activation and polarization after intracerebral haemorrhage.* Nat Rev Neurol, 2017. **13**(7): p. 420-433.
37. Guo, S., H. Wang, and Y. Yin, *Microglia Polarization From M1 to M2 in Neurodegenerative Diseases.* Front Aging Neurosci, 2022. **14**: p. 815347.

38. Neher, J.J., et al., *Phagocytosis executes delayed neuronal death after focal brain ischemia.* Proc Natl Acad Sci U S A, 2013. **110**(43): p. E4098-107.
39. Boada-Romero, E., et al., *The clearance of dead cells by efferocytosis.* Nat Rev Mol Cell Biol, 2020. **21**(7): p. 398-414.
40. Mike, J.K. and D.M. Ferriero, *Efferocytosis Mediated Modulation of Injury after Neonatal Brain Hypoxia-Ischemia.* Cells, 2021. **10**(5).
41. Wei, W., et al., *TREM2 regulates microglial lipid droplet formation and represses post-ischemic brain injury.* Biomed Pharmacother, 2024. **170**: p. 115962.
42. Yang, J., et al., *Interaction Between Microglial Lipid Droplet Metabolism and Immune Polarisation After Stroke: Mechanisms and Therapeutic Prospects.* Cell Mol Neurobiol, 2025. **46**(1): p. 10.
43. Lv, J., et al., *Examining the Impact of Microglia on Ischemic Stroke With an Emphasis on the Metabolism of Immune Cells.* CNS Neurosci Ther, 2025. **31**(2): p. e70229.
44. Kawabori, M. and M.A. Yenari, *The role of the microglia in acute CNS injury.* Metab Brain Dis, 2015. **30**(2): p. 381-92.
45. Shichita, T., H. Ooboshi, and A. Yoshimura, *Neuroimmune mechanisms and therapies mediating post-ischaemic brain injury and repair.* Nat Rev Neurosci, 2023. **24**(5): p. 299-312.
46. Soares, E., et al., *Neuroinflammation in Ischemic Stroke: Mechanisms, Systemic Interactions, and Therapeutic Targets.* Transl Stroke Res, 2026. **17**(3).
47. Kanazawa, M., et al., *Microglia and Monocytes/Macrophages Polarization Reveal Novel Therapeutic Mechanism against Stroke.* Int J Mol Sci, 2017. **18**(10).
48. Fan, P.L., et al., *Time-dependent dual effect of microglia in ischemic stroke.* Neurochem Int, 2023. **169**: p. 105584.
49. Candelario-Jalil, E., R.M. Dijkhuizen, and T. Magnus, *Neuroinflammation, Stroke, Blood-Brain Barrier Dysfunction, and Imaging Modalities.* Stroke, 2022. **53**(5): p. 1473-1486.
50. Qin, C., et al., *Dual Functions of Microglia in Ischemic Stroke.* Neurosci Bull, 2019. **35**(5): p. 921-933.
51. Han, M., et al., *Mesenchymal stem cell-derived extracellular vesicles promote microglial M2 polarization after subarachnoid hemorrhage in rats and involve the AMPK/NF-κB signaling pathway.* Biomed Pharmacother, 2021. **133**: p. 111048.
52. Mao, S., et al., *Extracellular vesicles enriched with miR-486 from Tetramethylpyrazine-preconditioned bone marrow mesenchymal stem cells promote microglia/macrophage M2 polarization and enhance neurogenesis in rats with ischemic stroke.* Stem Cell Res Ther, 2025. **16**(1): p. 455.
53. Zhu, H., et al., *Janus Kinase Inhibition Ameliorates Ischemic Stroke Injury and Neuroinflammation Through Reducing NLRP3 Inflammasome Activation via JAK2/STAT3 Pathway Inhibition.* Front Immunol, 2021. **12**: p. 714943.
54. Li, L., et al., *Astragaloside IV promotes microglia/macrophages M2 polarization and enhances neurogenesis and angiogenesis through PPARγ pathway after cerebral ischemia/reperfusion injury in rats.* Int Immunopharmacol, 2021. **92**: p. 107335.

55. Huang, R., et al., *PPARγ in Ischemia-Reperfusion Injury: Overview of the Biology and Therapy.* Front Pharmacol, 2021. **12**: p. 600618.
56. Tahmasebi, F. and S. Barati, *The Role of Microglial Depletion Approaches in Pathological Condition of CNS.* Cell Mol Neurobiol, 2023. **43**(6): p. 2459-2471.
57. Ma, Y., et al., *The Role of Immune Cells in Post-Stroke Angiogenesis and Neuronal Remodeling: The Known and the Unknown.* Front Immunol, 2021. **12**: p. 784098.
58. Bernardi, L.P., et al., *Microglial Responses to MSC-EVs Treatment in Animal and Cellular Models of Ischemic Stroke: a Systematic Review with Meta-analysis.* Mol Neurobiol, 2025. **62**(11): p. 14834-14857.
59. Haupt, M., S.T. Gerner, and T.R. Doeppner, *The dual role of microglia in ischemic stroke and its modulation via extracellular vesicles and stem cells.* Neuroprotection, 2024. **2**(1): p. 4-15.
60. Tian, T., et al., *Targeted delivery of neural progenitor cell-derived extracellular vesicles for anti-inflammation after cerebral ischemia.* Theranostics, 2021. **11**(13): p. 6507-6521.
61. Chuang, S.T., et al., *Enhancing CAR Macrophage Efferocytosis Via Surface Engineered Lipid Nanoparticles Targeting LXR Signaling.* Adv Mater, 2024. **36**(19): p. e2308377.
62. Im, S.S. and T.F. Osborne, *Liver x receptors in atherosclerosis and inflammation.* Circ Res, 2011. **108**(8): p. 996-1001.
63. Yeh, F.L., D.V. Hansen, and M. Sheng, *TREM2, Microglia, and Neurodegenerative Diseases.* Trends Mol Med, 2017. **23**(6): p. 512-533.
64. Deczkowska, A., A. Weiner, and I. Amit, *The Physiology, Pathology, and Potential Therapeutic Applications of the TREM2 Signaling Pathway.* Cell, 2020. **181**(6): p. 1207-1217.
65. Zhai, Q., et al., *Triggering Receptor Expressed on Myeloid Cells 2, a Novel Regulator of Immunocyte Phenotypes, Confers Neuroprotection by Relieving Neuroinflammation.* Anesthesiology, 2017. **127**(1): p. 98-110.
66. Zhu, L., et al., *FGF20 alleviates neuroinflammation in ischemic stroke by modulating microglial polarization via TREM2-TLR4/NF-κB pathway.* Cell Immunol, 2026. **423-424**: p. 105095.
67. Ri, M.H., et al., *Regulatory mechanisms of natural compounds from traditional Chinese herbal medicines on the microglial response in ischemic stroke.* Phytomedicine, 2023. **116**: p. 154889.
68. Wei, W., et al., *Dynamic Brain Lipid Profiles Modulate Microglial Lipid Droplet Accumulation and Inflammation Under Ischemic Conditions in Mice.* Adv Sci (Weinh), 2024. **11**(41): p. e2306863.
69. Huang, J., et al., *Interplay between lipid metabolism and macrophage dynamics in ischemic stroke: From mechanistic insights to therapeutic strategies.* Int Immunopharmacol, 2026. **169**: p. 115990.
70. Jaitin, D.A., et al., *Lipid-Associated Macrophages Control Metabolic Homeostasis in a Trem2-Dependent Manner.* Cell, 2019. **178**(3): p. 686-698.e14.
71. Krasemann, S., et al., *The TREM2-APOE Pathway Drives the Transcriptional Phenotype of Dysfunctional Microglia in Neurodegenerative Diseases.* Immunity, 2017. **47**(3): p. 566-581.e9.

72. Nugent, A.A., et al., *TREM2 Regulates Microglial Cholesterol Metabolism upon Chronic Phagocytic Challenge.* Neuron, 2020. **105**(5): p. 837-854.e9.

Figures

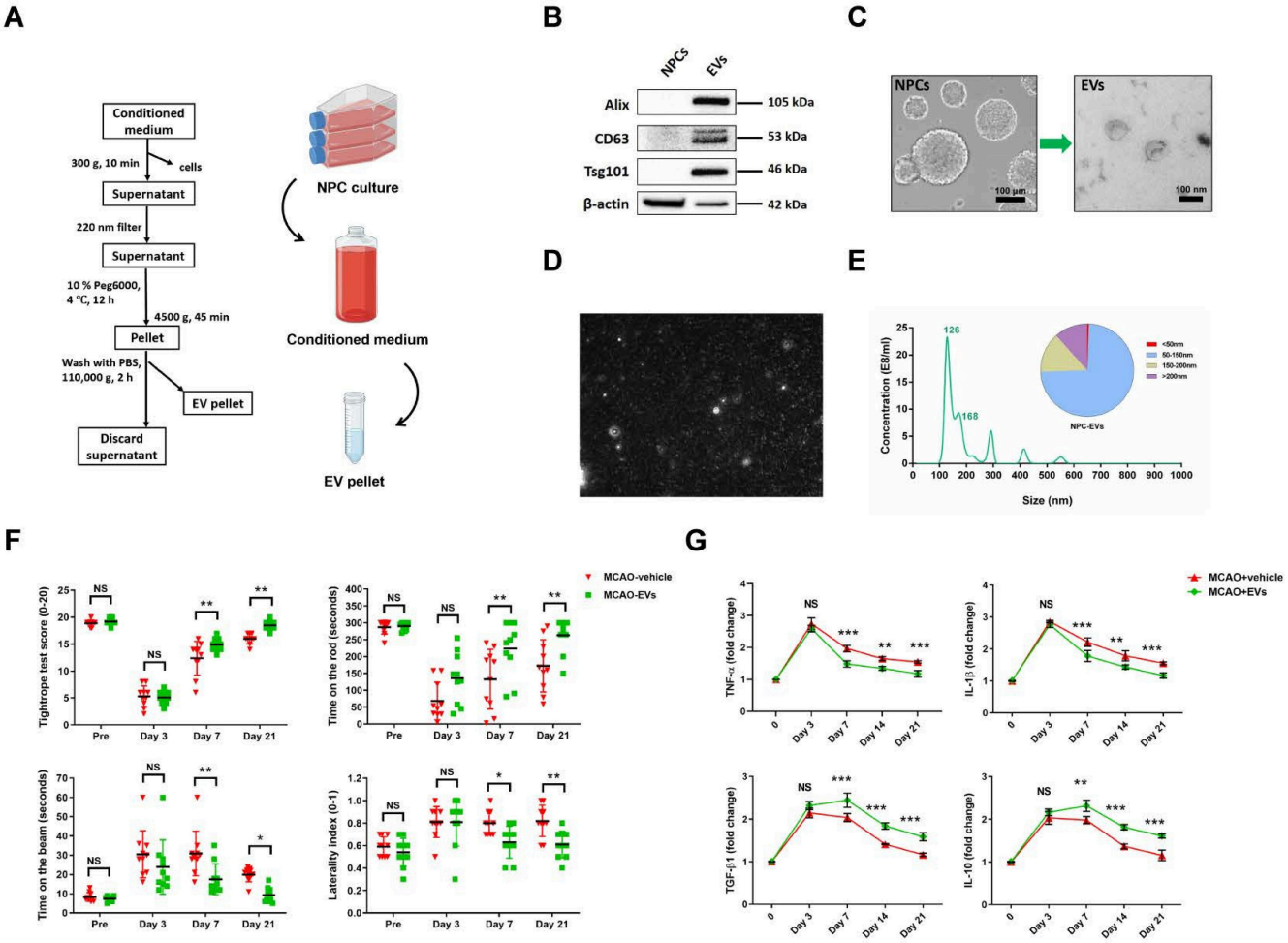


Figure 1

Extracellular vesicles (EVs) derived from NPCs (NPC-EVs) improved neurological recovery and induced anti-inflammation after stroke.

In the in vivo model, treated with NPC-EVs demonstrated enhanced neurological recovery following ischemic stroke, evidenced by improved neurobehavioral outcomes and increased anti-inflammatory cytokines. (A) In the schematic diagram, EVs were enriched from conditioned medium of NPCs by differential centrifugation. Resuspended EV precipitation enriched by polyethylene glycol 6000 were allowed to further enrich by ultracentrifugation. (B) Western blot analysis of EVs against exosomal markers such as CD63, Tsg101, and Alix, with β-actin serving as a loading control. Western blots were

performed on total cell lysates (CL) and EV lysates. (C) Representative optical microscope of NPCs (Scale bar: 100 μm), and representative transmission electron microscopy (TEM) analysis of EVs (cup-shaped EVs, scale bar: 200 nm). (D-E). Representative capture image displaying EV particle motion in nanoparticle tracking analysis (NTA), and the statistical diagram depicting size distribution patterns with peaks at 126 nm (EVs). (F) To evaluate the effect of EV administration on post-ischemic motor coordination impairment, the rotarod test, balance beam test, tightrope test, and corner turn test were done on day 1 before stroke (pre) as well as 3, 7 and 21 days after stroke in the C57BL/6 mice after stroke (n=10 per group). (G) Quantitative measurement of TNF-α, IL-β1, TGF-β1, and IL-10 levels of cerebral tissue homogenate in the vehicle or EV administration on day 1 before stroke (pre) as well as 3, 7, 14 and 21 days after stroke in the C57BL/6 mice (n=3 per group). Data are expressed as mean ± SD. NS: no significance, *p < 0.05, **p < 0.01, and ***p < 0.001. Abbreviations: IS, ischemic stroke; MCAO, middle cerebral artery occlusion; EVs, extracellular vesicles.

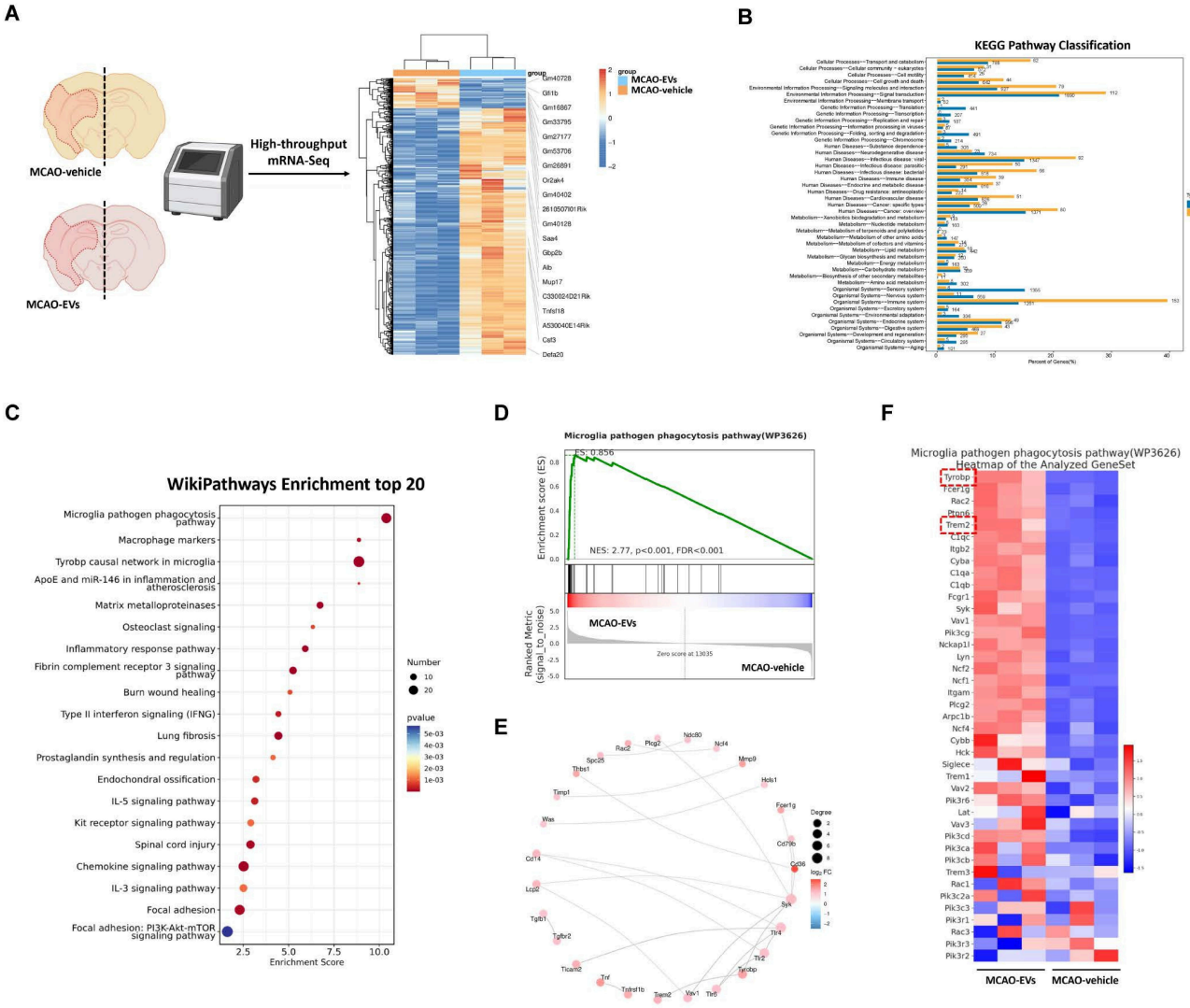


Figure 2

Transcriptomic analysis of cerebral tissue homogenate after EV administration in stroke mice.

In the MCAO in vivo model, RNA sequencing of tissues from the ischemic region revealed significant differences in the expression of immune and inflammation-related genes in EVs treated mice compared to vehicle treated controls. Pathway enrichment analysis highlighted potential regulatory mechanisms associated with microglial phagocytic function. Notably, heatmap analysis identified elevated expression of TREM2 as a potential key target involved in the modulation of microglial phagocytic activity. (A) Samples were collected from the ipsilateral side of the lesion in both the vehicle treated controls (MCAO-vehicle) and EVs treated groups (MCAO-EVs), followed by a preliminary comparative transcriptomic analysis. (B) Pathway expression analysis identified pathways exhibiting significant differential expression in immune and inflammation-related pathways between the two groups. (C-E) Mutual information analysis was used to compare the association between inflammation and microglial pathogen phagocytic functional gene signatures in samples from the MCAO-vehicle and MCAO-EVs groups. (F) The heatmap of the core region illustrates the relative differences in gene expression, with color-coded Z-scores representing the distribution of differential expression. Analysis of the heatmap revealed that the elevated expression of Trem2 and Tyrobp/DAP12 may serve as a critical target for the regulation of microglial phagocytic function. Abbreviations: IS, ischemic stroke; MCAO, middle cerebral artery occlusion; EVs, extracellular vesicles.

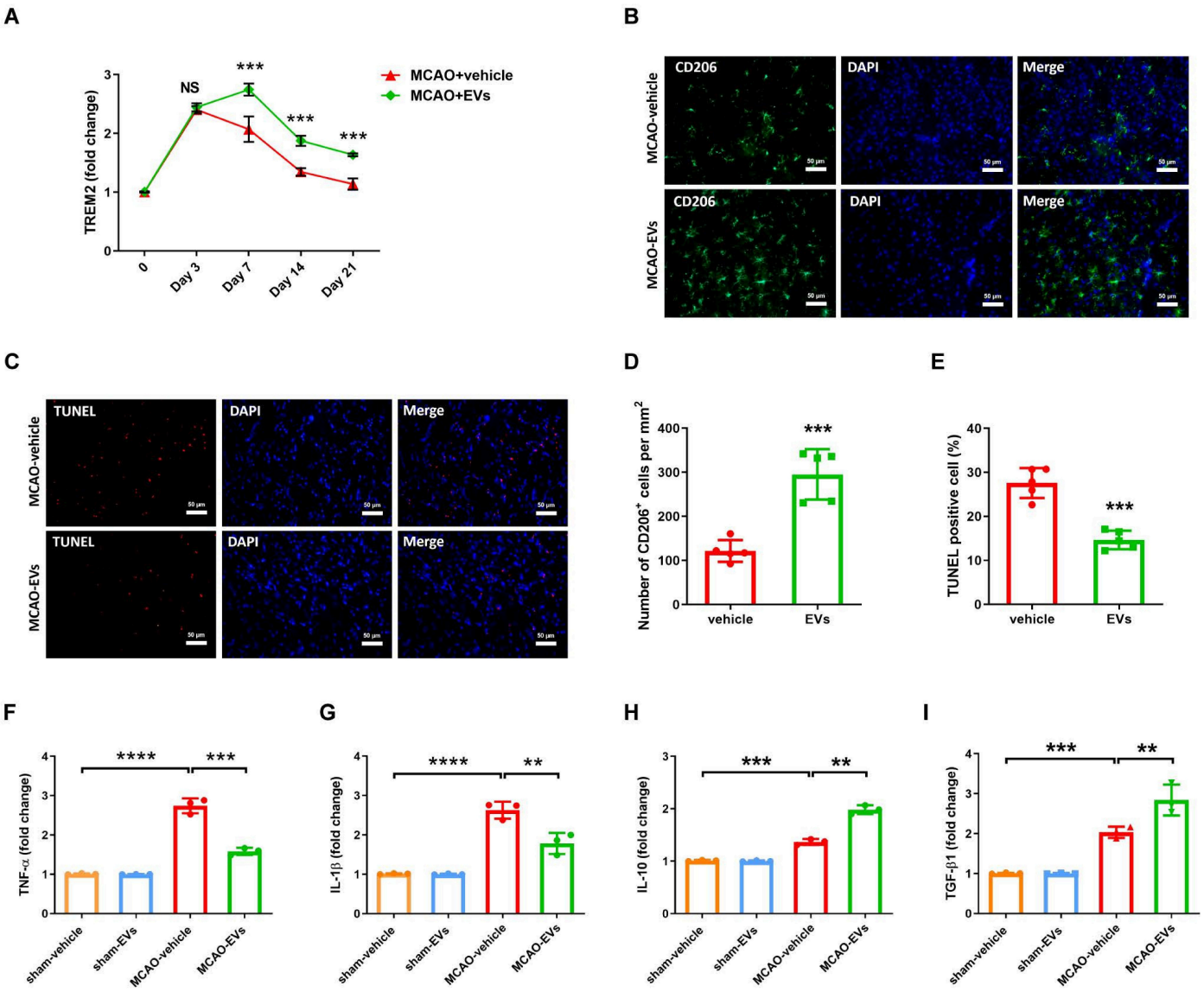


Figure 3

NPC-EVs drived microglia towards an M2-like phenotype and reduced neuronal apoptosis by promoting anti-inflammation in the MCAO stroke mice model.

In the in vivo model, EV administration facilitated M2 anti-inflammatory polarization and attenuated neuroinflammatory responses within the infarct region. (A) Quantitative measurement of TREM2 level of cerebral tissue homogenate in the vehicle or EV administration on day 1 before stroke (pre) as well as 3, 7, 14 and 21 days after stroke in the C57BL/6 mice after stroke (n=3 per group). (B, D) Representative fluorescence stainings and quantitative analysis of M2 microglia (CD206+, green) rates in the infarct area by immunohistochemical staining at post-MCAO day 7 in the vehicle control or EV administration. Scale bars: 50 μm (n=5 per group). (C, E) Representative immunofluorescence stainings and quantitative analysis of apoptotic cells (red) per mm^2 in the ischemic striatum at post-MCAO day 7 by TUNEL

staining in the vehicle control or EV administration (n=5 per group). Scale bars: 50 μm. (F-I) Summary of TNFα, IL-1β, IL-10, and TGF-β1 mRNA expression in the four groups (sham surgery with vehicle control; sham surgery with EV administration; MCAO with vehicle control; MCAO with EV administration) using qRT-PCR, normalized using the housekeeping gene β-actin (n=3). mRNA expression ratio in the sham surgery with vehicle control group was defined as 100 %. Data are expressed as mean ± SD. **p < 0.01, ***p < 0.001, ****p < 0.0001. Abbreviations: EVs, extracellular vesicles; TREM2, triggering receptor expressed on myeloid Cells 2; MCAO, middle cerebral artery occlusion; qRT-PCR, quantitative real-time polymerase chain reaction; TUNEL, terminal deoxynucleotidyl transferase dUTP nick end labeling.

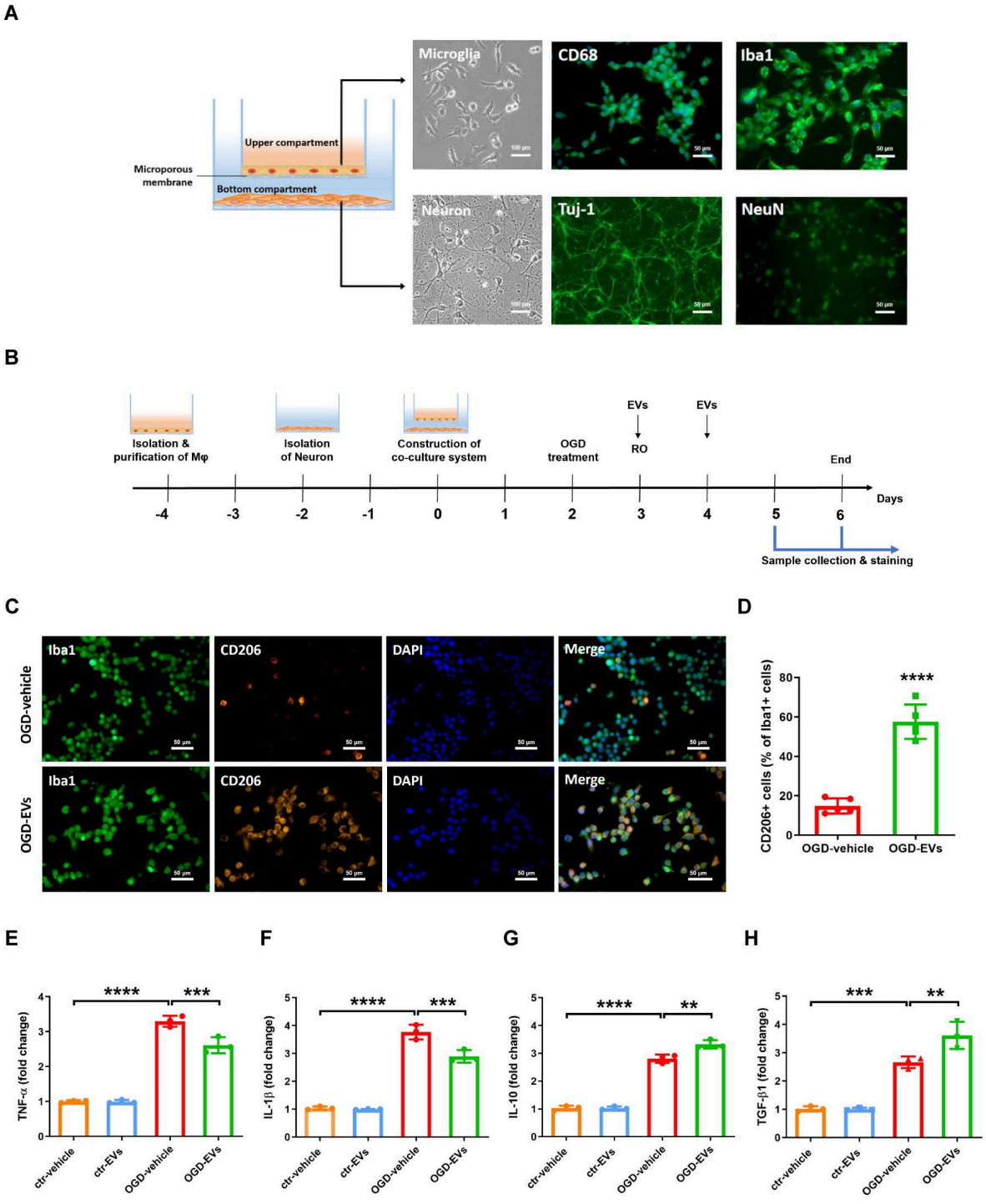


Figure 4

NPC-EVs increased anti-inflammation and induced microglial M2 polarization in the co-culture OGD model.

In an in vitro microglia-neuron co-culture model, NPC-EV treatment exhibited enhanced microglial M2 polarization, reduced secretion of extracellular pro-inflammatory factors, and increased production of

anti-inflammatory mediators following OGD/RO exposure. (A) The co-culture in vitro system consisted of primary microglia on a transwell insert with a microporous membrane and neurons on the other side. Scale bars: 100 μm. Immunofluorescence staining of their specific markers, CD68, Iba1 (microglia), Tuj-1, and NeuN (neuron) is depicted separately. Scale bars: 50 μm. (B) Experimental paradigm summarizing the in vitro microglia/neuron co-culture OGD model, including the preparation of microglia/neurons, construction of the co-culture system, and OGD/RO treatment. (C-D) Immunofluorescence of Iba1 in primary microglia (green) co-localized with CD206 (red). Quantitative analysis representing M2 polarization of microglia kept in the co-culture system consisted of the microglia treated with vehicle or EVs after OGD/RO treatment (n=5). Scale bars: 50 μm. (E-H) Quantitative measurement of IL-β1, TNF-α, IL-10, and TGF-β1 levels in the co-culture system treated with the vehicle or EVs after OGD/RO treatment using ELISA assay (n=6). Data are expressed as mean ± SD, ***$p < 0.001$, ****$p < 0.0001$. Abbreviations: EVs, extracellular vesicles; OGD, oxygen glucose deprivation; RO, reoxygenation.

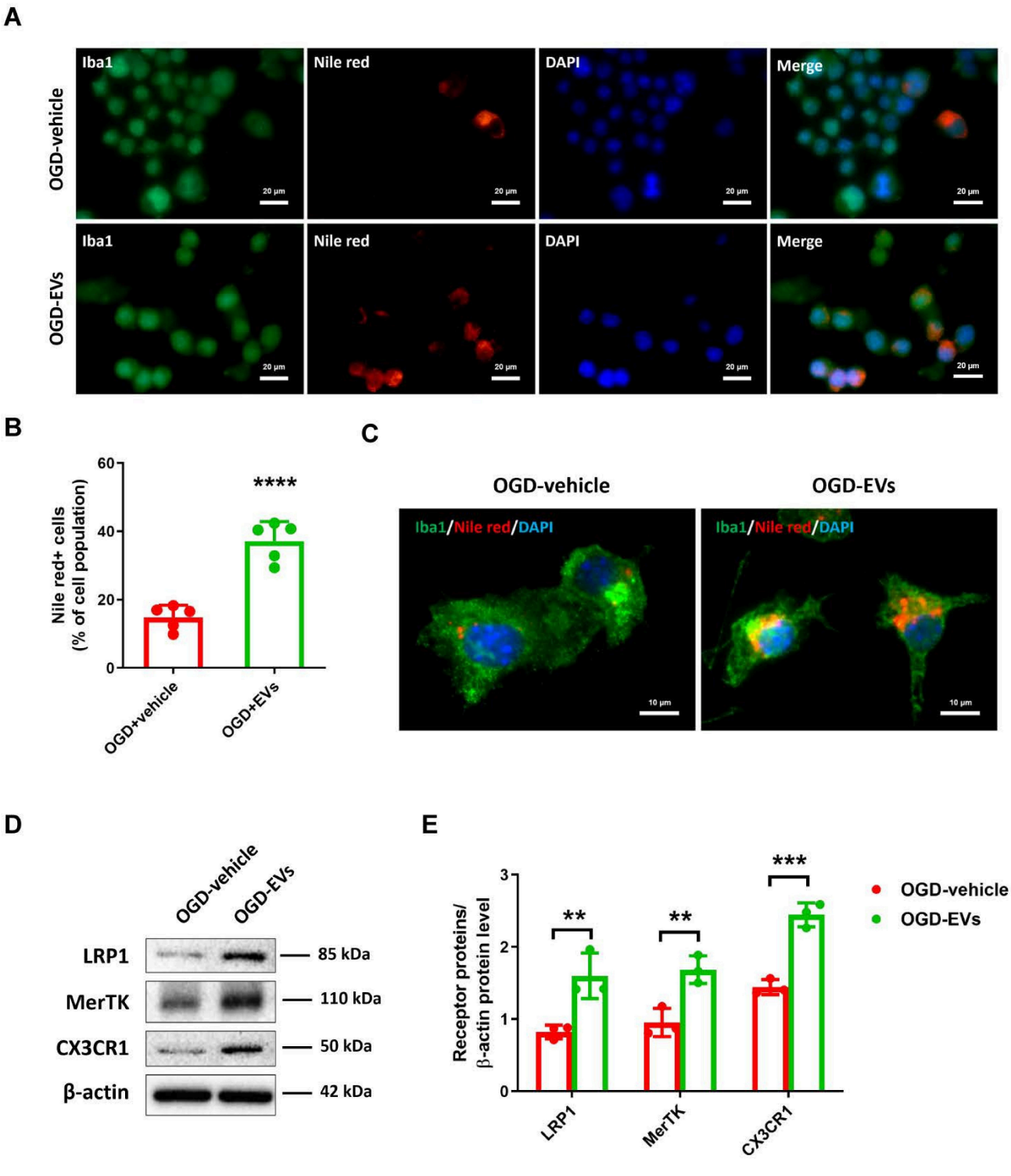


Figure 5

NPC-EVs facilitated microglial phagocytosis in the co-culture OGD model.

In an in vitro microglia-neuron co-culture model, NPC-EV-treated microglia demonstrated enhanced phagocytic activity and a significant upregulation of phagocytosis-related proteins following OGD/RO exposure. (A) The photos display representative immunofluorescence stainings of Iba1 (microglial

marker, green) and endocytic Nile red fluorescent microspheres (red) in the microglia treated with the vehicle or EVs. Scale bars: 20 μm. (B) Quantitative analysis of endocytic Nile red fluorescent microspheres (red) rate in same above groups (n=5 per group). (C) Amplified representative immunofluorescence stainings with higher resolution of Iba1 (microglial marker, green) and endocytic Nile red fluorescent microspheres (red) in the groups above. Scale bars: 10 μm. (D-E) Representative blots and quantitative analysis of efferocytotic process-dependent proteins, including LRP1, MerTK, and CX3CR1, in same above groups using Western blot analysis normalized with the housekeeping protein β-actin (n=3 per group). Data are expressed as mean ± SD. **p < 0.01, ***p < 0.001 and ****p < 0.0001. Abbreviations: EVs, extracellular vesicles; OGD, oxygen glucose deprivation; RO, reoxygenation.

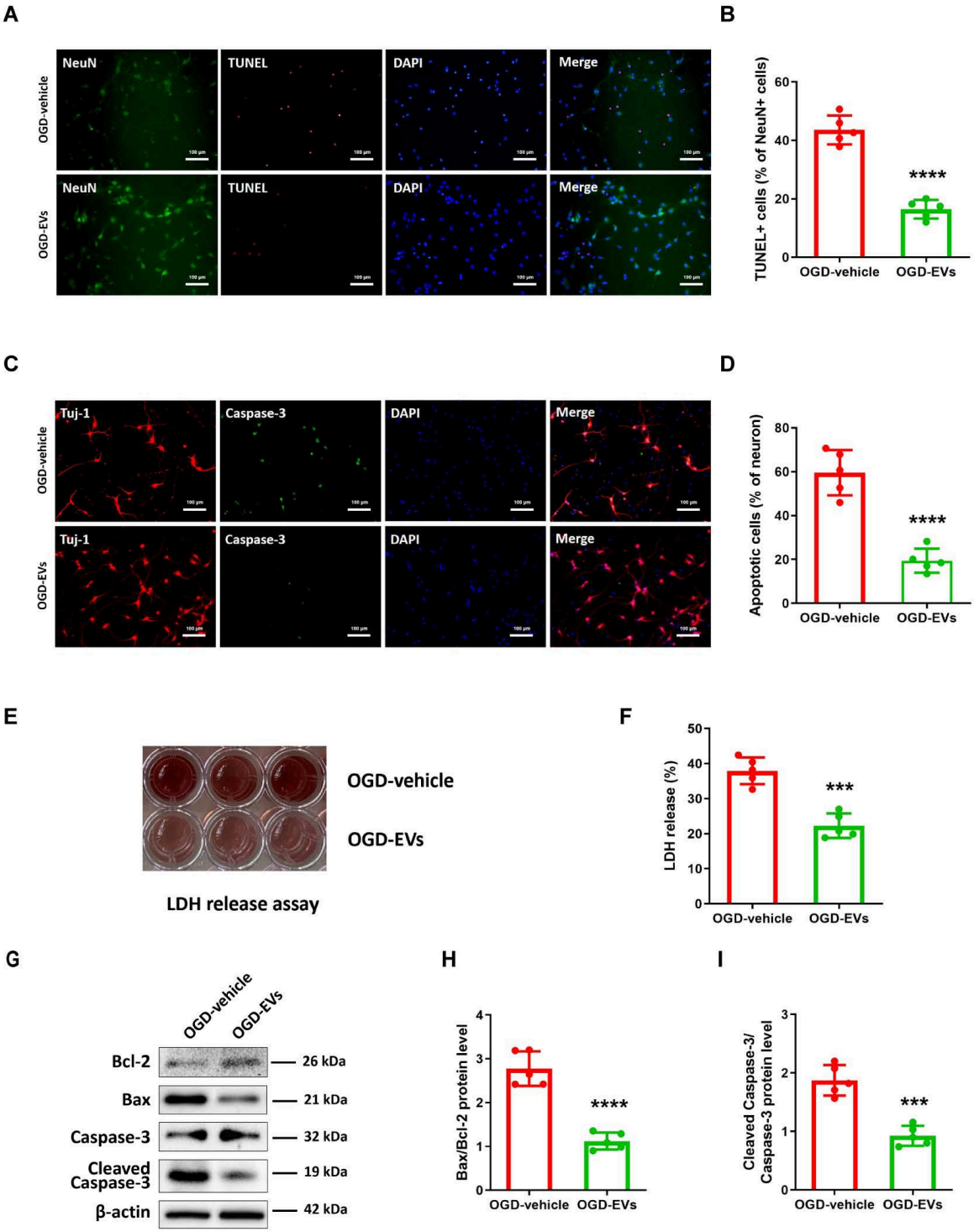


Figure 6

NPC-EVs attenuated apoptosis and cytotoxicity of neuronal cells in the co-culture OGD model.

In an in vitro microglia-neuron co-culture model, NPC-EV treated microglia, following OGD/RO exposure, reduced neuronal apoptosis rates, decreased cytotoxicity, and downregulated the expression of apoptosis-related proteins in response to neuronal injury. (A-B) Representative fluorescence staining and

analysis of apoptotic cell rates in cortical neurons (NeuN, green) by TUNEL staining (red) in the co-culture system treated with the vehicle or EVs. Scale bars: 100 μm (n=5 per group). (C-D) Representative immunofluorescence stainings and quantitative analysis of apoptotic-related protein caspase-3 (green) rate in primary cortical neurons (Tuj-1, red) in the groups above. Scale bars: 100 μm (n=5 per group). (E, F) Representative photo and quantitative analysis of OGD-induced neuronal cytotoxicity by using the LDH release assay (n=5) in the aforementioned groups. (G) Representative blots of apoptotic process-dependent proteins, including Bax, Bcl-2, cleaved caspase-3, and caspase-3 in the above same groups using Western blot analysis normalized with the housekeeping protein β-actin. (H-I) Quantitative analysis of the ratio of Bax/Bcl-2 and cleaved caspase-3/caspase-3 in neurons co-cultured with the vehicle or EV treated microglia after OGD/RO treatment (n=3 per group). Data are expressed as mean ± SD. ***$p < 0.001$ and ****$p < 0.0001$. Abbreviations: OGD, oxygen glucose deprivation; RO, reoxygenation; EVs, extracellular vesicles; LDH, lactate dehydrogenase; TUNEL, terminal deoxynucleotidyl transferase dUTP nick end labeling.

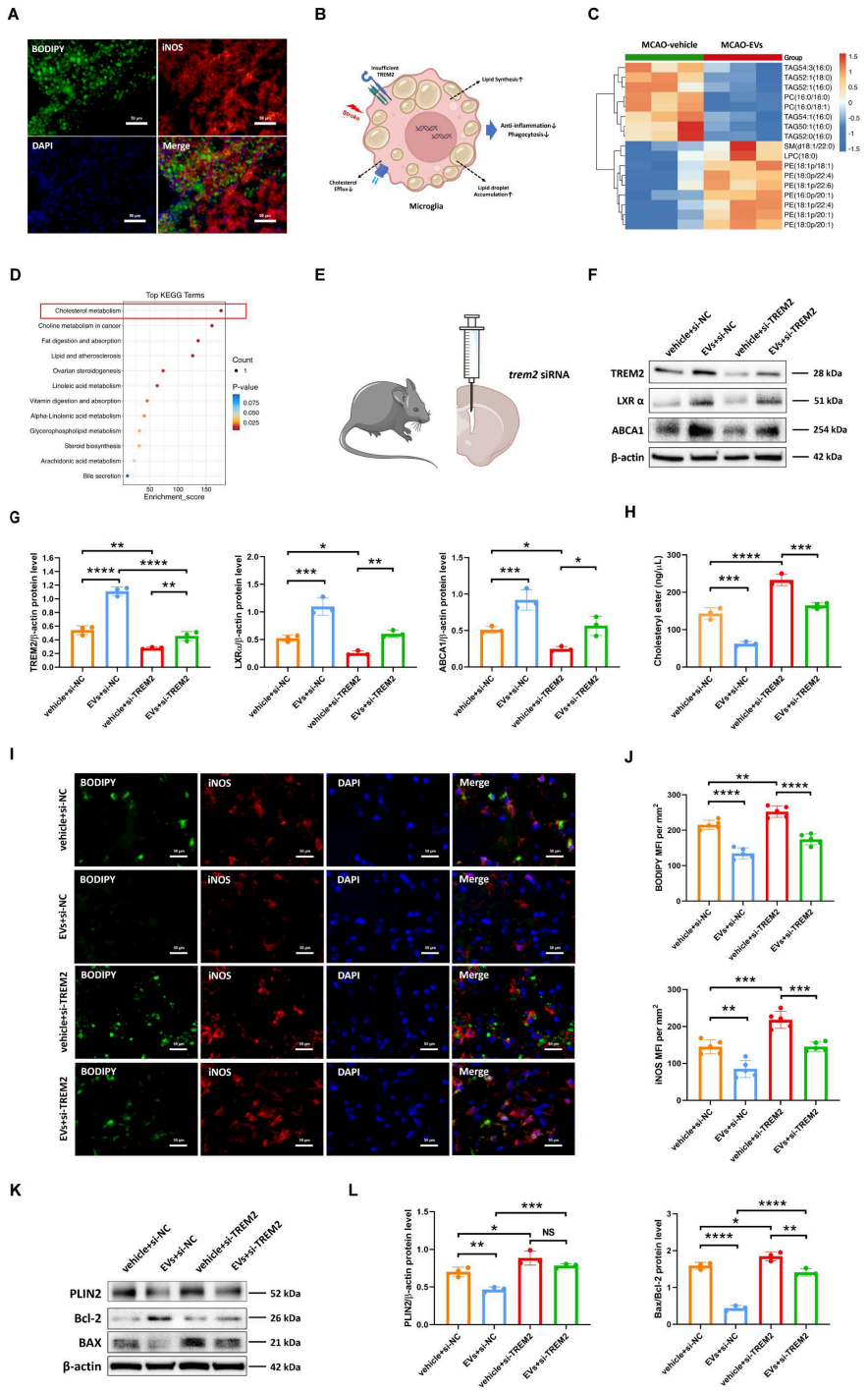


Figure 7

The role of TREM2 in modulating microglial function and lipid metabolism alterations in the NPC-EV treated mouse model after stroke.

In ischemic stroke model, NPC-EV administration upregulated TREM2 expression, suppressed microglial pro-inflammatory polarization, reduced lipid microsome accumulation, and inhibited neuronal apoptosis.

(A) Representative fluorescence staining of lipid droplet (BODIPY, green) in pro-inflammatory microglia (iNOS, red) in the infarct area by immunohistochemical staining at post-MCAO day 7. Scale bars: 50 μm (n=5 per group). (B) In the schematic diagram, insufficient TREM2 in ischemic brain, accompanied by increased lipid accumulation and decreased cholesterol efflux, impaired microglial function including anti-inflammation and phagocytosis. (C-D) Lipidomic analysis revealed that NPC-EV administration significantly altered lipid metabolism, especially cholesterol metabolism in microglia. (E) In the schematic diagram, trem2 or negative control si-RNA (si-TREM2 or si-NC) was delivered to lateral ventricle knocking down the corresponding gene by stereotactic injection in stroke mice. (F-G) Representative blots and quantitative analysis of the TREM2 expression in the four groups (vehicle with si-NC injection; EVs with si-NC injection; vehicle with si-TREM2 injection; EVs with si-TREM2 injection) using Western blot analysis normalized with the housekeeping protein β-actin (n=3 per group). (H) Quantification of the level of cholesteryl ester in the same four groups (n=3 per group). (I-J). Representative immunofluorescence stainings and quantitative analysis of BODIPY (green) rate in activated microglia (iNOS, red) in the four different groups. Scale bars: 100 μm (n=5 per group). (K-L) Quantitative analysis of the ratio of Bax/Bcl-2 and PLIN2 expression in the groups above after MCAO treatment (n=3 per group). Data are expressed as mean ± SD. *$p < 0.05$, **$p < 0.01$, ***$p < 0.001$ and ****$p < 0.0001$. Abbreviations: MCAO, middle cerebral artery occlusion; EVs, extracellular vesicles; NC, negative control.

Supplementary Files

This is a list of supplementary files associated with this preprint. Click to download.

- SupplementaryMaterials.docx
- floatimage1.jpeg